

Article

Thermal Stability of NASICON-Type $\text{Na}_3\text{V}_2(\text{PO}_4)_3$ and $\text{Na}_4\text{VMn}(\text{PO}_4)_3$ as Cathode Materials for Sodium-ion Batteries

Ruslan R. Samigullin ^{1,*}, Maxim V. Zakharkin ¹, Oleg A. Drozhzhin ^{1,*} and Evgeny V. Antipov ^{1,2}¹ Department of Chemistry, Lomonosov Moscow State University, 119991 Moscow, Russia² Skoltech Center for Energy Science and Technology, Skolkovo Institute of Science and Technology, 143026 Moscow, Russia

* Correspondence: ruslan.samigullin@chemistry.msu.ru (R.R.S.); drozhzhin@elch.chem.msu.ru (O.A.D.)

Abstract: The thermal stability of NASICON-type cathode materials for sodium-ion batteries was studied using differential scanning calorimetry (DSC) and in situ high-temperature powder X-ray diffraction (HTPXRD) applied to the electrodes in a pristine or charged state. $\text{Na}_3\text{V}_2(\text{PO}_4)_3$ and $\text{Na}_4\text{VMn}(\text{PO}_4)_3$ were analyzed for their peak temperatures and the exothermic effect values of their decomposition processes, as well as the phase transformations that took place upon heating. The obtained results indicate that Mn-substituted cathode material demonstrates much poorer thermal stability in the charged state, although pristine samples of both materials exhibit similar thermal behavior without any DSC peaks or temperature-induced phase transitions in the studied temperature range. The in situ HTPXRD revealed the amorphization of desodiated $\text{Na}_4\text{VMn}(\text{PO}_4)_3$ -based electrodes occurring at 150~250 °C.

Keywords: thermal stability; DSC; HTPXRD; NASICON; substitution; cathode; sodium-ion battery



Citation: Samigullin, R.R.; Zakharkin, M.V.; Drozhzhin, O.A.; Antipov, E.V. Thermal Stability of NASICON-Type $\text{Na}_3\text{V}_2(\text{PO}_4)_3$ and $\text{Na}_4\text{VMn}(\text{PO}_4)_3$ as Cathode Materials for Sodium-ion Batteries. *Energies* **2023**, *16*, 3051. <https://doi.org/10.3390/en16073051>

Academic Editors: Bohayra Mortazavi and Meysam Makaremi

Received: 27 February 2023

Revised: 16 March 2023

Accepted: 25 March 2023

Published: 27 March 2023



Copyright: © 2023 by the authors. Licensee MDPI, Basel, Switzerland. This article is an open access article distributed under the terms and conditions of the Creative Commons Attribution (CC BY) license (<https://creativecommons.org/licenses/by/4.0/>).

1. Introduction

The rapid development of advanced energy storage technology is an important challenge in the 21st century [1]. Lithium-ion batteries (LIBs) became the headliner among other electrochemical systems (lead-acid, nickel-cadmium, nickel-metal hydride, etc.) since their first commercialization in 1991 due to their high energy density, excellent cyclability, absence of “memory effects”, low self-discharge rate and other features. As a result, most of the devices built today, i.e., portable gadgets, electrical vehicles (EVs) and grid energy storage systems, are operated by LIBs of different sizes and formats [2]. However, further implementation of mass storage systems for energy storage faces an ineluctable challenge that is linked to both lithium cost and its availability. Thus, in all likelihood, the proven reserves of lithium will not be enough to meet the needs of the electric vehicle and distributed energy industries in the coming decades [3].

Due to the low cost and widespread distribution of sodium, as well as its chemical properties, which are similar to lithium, sodium-ion batteries (SIBs) have been introduced as an alternative to LIBs, and they have attracted keen interest from battery researchers and manufacturers [4]. Furthermore, the cost of SIBs is additionally reduced due to the facts that aluminum can be used for both positive and negative current collectors and is cheaper, lighter and more abundant than the copper used in the negative current collectors of LIBs [5]. Thus, sodium-ion batteries (SIBs) are expected to become an alternative to lithium-ion batteries (LIBs) in transportation and large-scale utility grid applications [6–8]. Safety issues are especially challenging in these cases, since the average capacity of the systems vary between several MWh and GWh. The severity of battery failures depends on various factors, including the battery’s state of charge, ambient conditions and the battery’s mechanical and electrochemical design [9]. The reactivity of cathode materials at different states of charge is one of the aspects affecting battery safety. On the other hand, the common power capacity and diffusion rate of materials for SIBs are still among the main

obstacles that prevent their widespread use [10,11]. Moreover, since the radius of sodium (0.98 Å) is larger than that of lithium (0.69 Å), the large volume change caused by the extraction and insertion of sodium ions between the electrodes results in severe structural disturbances [12,13]. Thus, an extremely urgent problem is the search for materials that can provide a high electrochemical capacity, a good diffusion rate of sodium cations, small volume changes and high thermal stability [14].

Aiming to find reversible intercalation electrodes for rapid charge transfer, various host materials have been explored as a potential cathode material in state-of-the-art SIB's, including transition metal oxides [8,15], polyanionic materials [16] and Prussian blue analogues [17–19]. Among them, polyanionic materials with a NASICON-type structure attract significant interest as SIB cathodes due to their robust three-dimensional (3D) framework with large gap channels, which provides higher thermal and cycling stability than Prussian blue analogues or layered oxides [20–29]. One of the first [30] and most extensively studied NASICON-type cathode materials for SIBs is $\text{Na}_3\text{V}_2(\text{PO}_4)_3$ (NVP). It crystallizes in the trigonal system, e.g., $R\bar{3}c$ [31]. NASICON structures consist of corner-sharing PO_4 tetrahedra and VO_6 octahedra with sodium cations in interstitial positions. Through strong covalent bonds with phosphorus, all of the oxygen ions form PO_4 polyanions, which provide improved stability for the 3D framework as compared with other types of cathode materials. It is worth noting that the actual application of $\text{Na}_3\text{V}_2(\text{PO}_4)_3$ is always limited by its low inherent electronic conductivity, which results in low specific capability, poor cycling stability and poor rate performance. A number of efforts have been made to improve NVP's electrochemical performance through surface modifications, such as carbon coating [32,33] and doping [34–39]. Carbon-coated $\text{Na}_3\text{V}_2(\text{PO}_4)_3/\text{C}$ has been demonstrated to have long-term stability and exceptional performance when used as a cathode [40].

In situ and operando X-ray diffraction are powerful methods to investigate crystal structure transformations during heating or charging/discharging [41]. Thus, it was shown by means of in situ high-temperature X-ray diffraction (HTXRD) that Prussian blue (PB) analogues exhibit water release from their crystalline lattice, and further decomposition is based on the release of cyanogen gas from the structures, leading to a transformation of PB into cubic iron hexacyanoferrate and, finally, to the breakdown of the formed cubic structure [42,43]. Dai et al. studied the impact of sintering temperatures on the capacity and thermal behavior of honeycomb-ordered O3-type $\text{NaNi}_{2/3}\text{Sb}_{1/3}\text{O}_2$ cathode materials [44]. It was shown that the sample prepared at 950 °C exhibited the smallest charge-transfer resistance as well as the largest sodium ion diffusion coefficient, endowing this material with a stable discharge capacity and a decent cycling performance. Meanwhile, this material demonstrates excellent thermal stability up to 500 °C, as was found by means in situ HTXRD. As for phosphate cathode materials, $\text{Na}_3\text{V}_2(\text{PO}_4)_3$ has excellent thermal stability in its pristine and desodiated $\text{Na}_1\text{V}_2(\text{PO}_4)_3$ state and a temperature range of 25–450 °C, as shown by means of in situ HTPXRD [45]. In situ HTPXRD patterns of NASICON-type materials indexed in an $R\bar{3}c$ space group show that the c parameter increases with an increase in temperature, while the a parameter is almost temperature-independent, and, thus, the thermal expansion occurs along the c axis [46,47]. According to our previous work [29], the thermal decomposition effect of an $\text{Na}_3\text{V}_2(\text{PO}_4)_3$ -based electrode charged up to 4.1 V is $\sim 100 \text{ J g}^{-1}$, which is nearly three times lower than that of a charged $\text{NaNi}_{1/3}\text{Fe}_{1/3}\text{Mn}_{1/3}\text{O}_2$ -based electrode. Cui et al. [48] studied the thermal runaway behavior of the 500-mAh soft-packed symmetrical NVP//NVP and NVP//hard carbon batteries by means accelerating the rate calorimetry (ARC). The results indicate that the NVP//NVP symmetrical batteries have excellent prospects for application in special fields with high safety requirements. Moreover, the thermal stabilities of six kinds of electrolytes, charged NVPs and their mixture were investigated by TG and ARC [49]. The results obtained in this work also confirmed the high stability of the NVP-based cathodes.

The main drawback for the practical application of $\text{Na}_3\text{V}_2(\text{PO}_4)_3$ as a cathode material is its modest energy density ($\sim 350 \text{ Wh}\cdot\text{kg}^{-1}$) based on the $\text{V}^{4+}/\text{V}^{3+}$ redox at an average voltage of 3.4 V; therefore, great efforts of the scientific community are aimed at modifying

the composition of the material to increase its working potential and/or reversible capacity. The substitution of transition metal in the cathode materials of metal-ion batteries is a common method of increasing their energy density. Different NASICON-type materials with iso- or heterovalent substitutions of vanadium $\text{Na}_{3+\delta}\text{V}_{2-x}\text{M}_x(\text{PO}_4)_3$ ($\text{M} = \text{Ti}, \text{Cr}, \text{Mn}, \text{Fe}, \text{Co}$ and Ni) were explored [22]. In general, the replacement of V^{3+} with trivalent cations that are not electrochemically active or are not active at the typical working potentials activates the $\text{V}^{5+}/\text{V}^{4+}$ redox couple, which increases the average operating voltage [50–52]. Substituting vanadium with divalent metal cations not only activates the $\text{V}^{5+}/\text{V}^{4+}$ redox couple, but also causes an increase in the number of sodium ions in the NASICON structure [53]. A number of works show that manganese substitution in NASICON-type $\text{Na}_{3+x}\text{V}_{2-x}\text{Mn}_x(\text{PO}_4)_3$ ($0 \leq x \leq 1$) materials increases their average (dis)charge potential, rate capability and capacity [54–59]. Replacement of smaller V^{3+} cations with larger Mn^{2+} enhances the sodium content in the initial material and increases the unit cell volume. As in the case of $\text{Na}_3\text{V}_2(\text{PO}_4)_3$, only two Na^+ ions are extracted from $\text{Na}_4\text{VMn}(\text{PO}_4)_3$ in a charge to 3.8 V. In contrast to $\text{Na}_1\text{V}_2(\text{PO}_4)_3$, further Na^+ extraction from $\text{Na}_2\text{VMn}(\text{PO}_4)_3$ is realized through the $\text{V}^{5+}/\text{V}^{4+}$ redox at 3.9 V, which enhances both voltage and capacity. Moreover, the presence of Mn in the cation sublattice alters the phase transformation behavior and distribution of sodium cations over different positions at various stages of the charge-discharge cycle [60–63]. However, as a cathode material with good performance, the knowledge of the thermal stability of manganese-substituted NASICON-type materials is still lacking.

In this study, we demonstrate the negative effect of manganese substitution on the thermal stability of NASICON-type cathode materials for the first time. $\text{Na}_3\text{V}_2(\text{PO}_4)_3$ and $\text{Na}_4\text{VMn}(\text{PO}_4)_3$ were studied by means of DSC and HTXRD to examine their pristine and two-charged states (3.8 V and 4.5 V vs. Na/Na^+) and a temperature range of 25–450 °C.

2. Materials and Methods

2.1. Material Preparation

The $\text{Na}_4\text{VMn}(\text{PO}_4)_3$ was prepared by dissolving manganese(II) acetylacetonate, vanadium (V) oxide and citric acid in deionized water in a stoichiometric ratio and stirring for 40 min at 70 °C. Then sodium carbonate and ammonium dihydrophosphate solution in deionized water with a molar ratio of 4:3 were added drop-wise and stirred for 40 min, followed by evaporation at 95 °C overnight. Vanadium (V) oxide, citric acid and sodium dihydrophosphate were used to obtain the $\text{Na}_3\text{V}_2(\text{PO}_4)_3$ by the same procedure. After the solid residue was ground in a ball-mill, it was annealed at 750 °C for 8 h in an inert atmosphere.

To prepare the electrodes, all powders were mixed with Super P carbon (Timcal) and poly(vinylidene fluoride) (PVDF, Solef 5130, Solvay) in a weight ratio of 93:1:6 and dissolved in N-methyl-2-pyrrolidone (NMP). The resulting slurry was coated with aluminum foil. The cast sheet was dried at 80 °C to remove the NMP and then roll-pressed and punched into 10 or 16 mm diameter electrodes. Subsequently, the punched electrodes were dried at 120 °C under a vacuum and used for cell assembly.

2.2. Materials Characterization

Two-electrode cells were assembled using the $\text{Na}_3\text{V}_2(\text{PO}_4)_3$ and $\text{Na}_4\text{VMn}(\text{PO}_4)_3$ as the working electrodes, sodium metal (Sigma Aldrich) as the counter electrode and glass fiber as the separator for differential scanning calorimetry studies. A quantity of 1 M of NaPF_6 solution (Kishida Chemical) in a 1:1 vol. mixture of ethylene carbonate/propylene carbonate (EC/PC) was used as the electrolyte. Galvanostatic experiments were carried out using an Elins P-20X8 potentiostat-galvanostat (ES8 software).

Using a Netzsch DSC 204 F1 Phoenix instrument, differential scanning calorimetry was carried out within a 50–450 °C temperature range and with a heating rate of 5 °C min^{-1} in hermetically sealed high-pressure Cr-Ni stainless steel crucibles and in an argon atmosphere. Electrodes were extracted from fully charged “half-cells”, washed with DMC

and dried under vacuum. The dried electrode powders were placed in the crucibles. The crucibles with samples were hermetically sealed in a dry-argon glove box. To calculate the magnitude of the heat effect, we used the area under the peak on the DSC curve after subtracting the background (if any) using Netzsch Proteus software.

In situ high-temperature powder X-ray diffraction (HTPXRD) patterns were recorded with a Bruker D8 ADVANCE diffractometer equipped with the energy-dispersive LYNX-EYE position-sensitive detector within a 25–450 °C temperature range and with a heating rate of 0.1 °C s⁻¹ in a flowing argon atmosphere. The waiting time between heating and measurement was 200 s, and the scan speed was 0.2° min⁻¹ (Cu K_{α1,2} radiation, 6.5–30°, 40 kV, 40 mA).

Scanning Electron Microscopy (SEM) images were obtained with a JEOL JSM-6490LV electron microscope (tungsten hairpin electron gun, 30 kV) equipped with an Everhart-Thornley detector.

3. Results and Discussion

3.1. Structural and Morphological Aspects

Figure 1 shows the XRD patterns of the as-synthesized materials. It can be indexed in the well-known NASICON unit cell with the $R\bar{3}c$ space group with the following parameters: $a = 8.7307(2)$ Å, $c = 21.8203(7)$ Å, $V = 1440.42(7)$ Å³ for Na₃V₂(PO₄)₃, $a = 8.9727(1)$ Å, $c = 21.4500(4)$ Å and $V = 1495.58(4)$ Å³ for Na₄VMn(PO₄)₃. SEM images of the as-synthesized Na₃V₂(PO₄)₃ and Na₄VMn(PO₄)₃ cathode materials are presented in Figure 1. As one can see, the morphology of the samples is quite similar; smaller submicron-sized particles form larger aggregates of 5–10 μm.

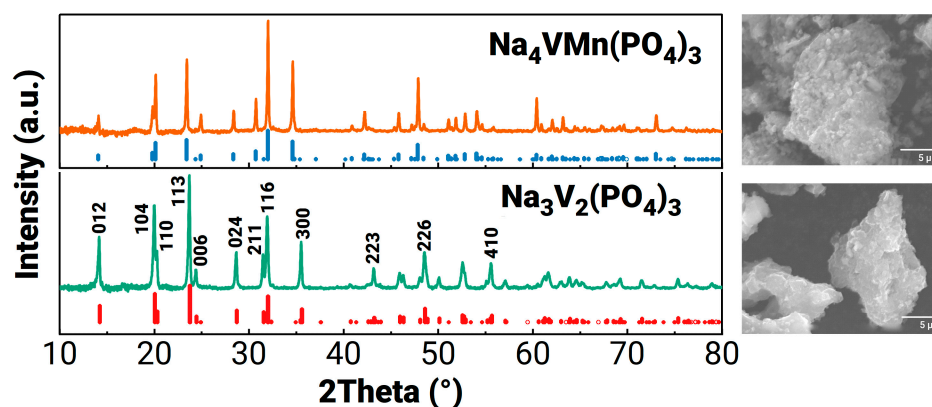


Figure 1. XRD patterns and SEM images of the as-synthesized Na₃V₂(PO₄)₃ (green) and Na₄VMn(PO₄)₃ (yellow) cathode materials. Theoretical peak positions and intensities are shown by red and blue bars, correspondingly.

3.2. Electrochemical Properties

Detailed electrochemical and structural properties of the materials have been reported previously [55,60,62,64] and, therefore, are not described in the present work. Briefly, Na₃V₂(PO₄)₃ always exhibits a capacity of 100–120 mAh·g⁻¹ (corresponding to reversible (de)intercalation of 2 Na⁺ per formula unit), regardless of the upper limit of the potential. In other words, it is impossible to extract more than two sodium cations from Na₃V₂(PO₄)₃ using electrochemical methods. The situation is different for Mn-substituted materials; they also exhibit reversible (de)intercalation of two sodium cations upon charge-discharge up to 3.8 V (vs. Na/Na⁺ hereinafter); however, if this limit is increased, additional Na⁺ can be extracted. As a result, the subsequent electrochemical properties of the material change drastically. We decided to study, firstly, the effect of manganese substitution on the stability of NASICON-type structures and, secondly, how thermal stability is affected by the extraction of more than two sodium cations from the unit cell.

To analyze the thermal stability of the materials in a charged state, all electrodes were charged up to 3.8 V and 4.5 V potentials at C/10 current densities in a sodium half-cell. Corresponding voltage curves are presented in Figure 2. As the figure illustrates, the charging capacity of the $\text{Na}_3\text{V}_2(\text{PO}_4)_3$ essentially does not change with an increase in the upper limit of the potential from 3.8 to 4.5 V (except for a small increase, apparently associated with the formation of CEI). On the other hand, the $\text{Na}_4\text{VMn}(\text{PO}_4)_3$ demonstrates an increase in capacity from 100 to 150 $\text{mAh}\cdot\text{g}^{-1}$, which is in good agreement with the data obtained in previous work [60] and summarized above.

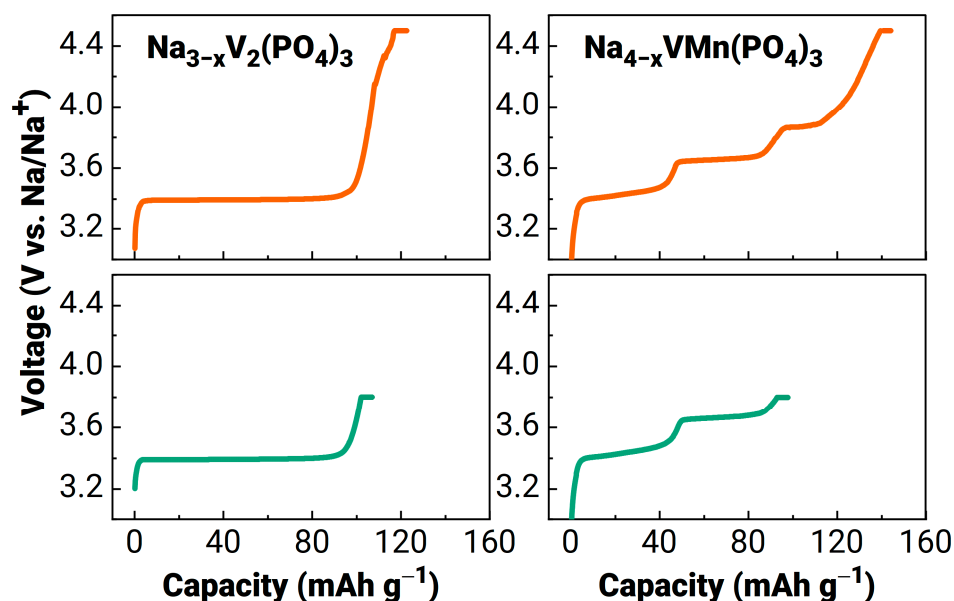


Figure 2. Charged curves of $\text{Na}_3\text{V}_2(\text{PO}_4)_3$ and $\text{Na}_4\text{VMn}(\text{PO}_4)_3$ cathode materials at different potential cut-offs (3.8 V on the **bottom** and 4.5 V on the **top**).

3.3. Differential Scanning Calorimetry

Figure 3 shows the DSC curves of the pristine powders of all of the samples. The $\text{Na}_3\text{V}_2(\text{PO}_4)_3$ (NVP) exhibits two endothermic peaks at $\sim 60^\circ\text{C}$ and $\sim 175^\circ\text{C}$, which indicate $\alpha\text{-NVP} \rightarrow \beta\beta'\text{-NVP} \rightarrow \gamma\text{-NVP}$ polymorph transformations [65]. In contrast, the manganese-substituted material exhibits only one endothermic peak at $\sim 55\text{--}65^\circ\text{C}$, which implies only a single polymorph transformation. These data allow us to recognize the original phosphates as thermally stable materials, at least within the studied temperature range.

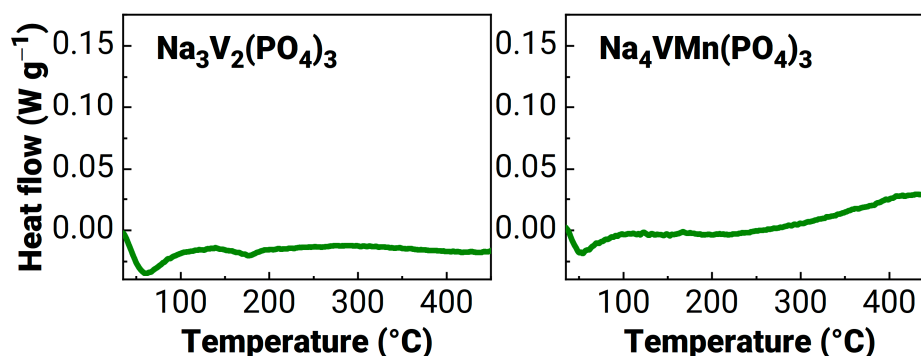


Figure 3. DSC curves for the pristine powders of $\text{Na}_3\text{V}_2(\text{PO}_4)_3$ and $\text{Na}_4\text{VMn}(\text{PO}_4)_3$ cathode materials.

The DSC curves of the charged, washed and dried electrodes are presented in Figure 4. The $\text{Na}_3\text{V}_2(\text{PO}_4)_3$, electrochemically desodiated at 3.8 V, shows an exothermic peak at

415 °C (with an onset temperature of 347 °C) and an enthalpy of 78 J g⁻¹. Charging the Na₃V₂(PO₄)₃ up to a higher potential of 4.5 V decreased the onset temperature by 10 °C (to 337 °C) and the peak temperature by 30 °C (to 385 °C.) The exothermic effect, in this case, amounted to 151 J g⁻¹, which was approximately two times higher than that for the electrode charged up to 3.8 V (Table 1). However, as demonstrated in Figure 4, the exothermic effect signals were “distributed” within the temperature range, which is most probably a result of a surface reaction with PVDF or cathode–electrolyte interphase (CEI) components [66], while the intensities of the peaks at ~400 °C were nearly equal. More reactive CEI components can be formed due to the high charge potential (4.5 V) that nears the stability limit of alkyl carbonate electrolytes for sodium-ion batteries.

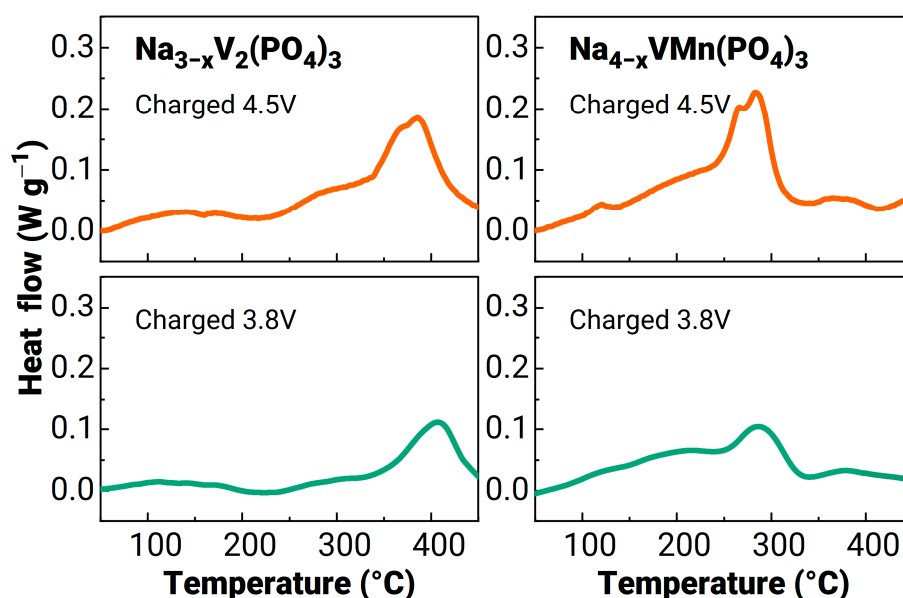


Figure 4. DSC curves for the charged electrodes containing Na₃V₂(PO₄)₃ and Na₄VMn(PO₄)₃ cathode materials at different potential cut-offs (3.8 V on the **bottom** and 4.5 V on the **top**).

Table 1. Differential Scanning Calorimetry Data.

Sample	Peak Temperature, °C	Enthalpy, J g ⁻¹	HoE Factor
Na ₃ V ₂ (PO ₄) ₃	3.8 V	415	78
	4.5 V	370, 385	151
Na ₄ VMn(PO ₄) ₃	3.8 V	287	163
	4.5 V	266, 283	239

In turn, the Na_{4-x}VMn(PO₄)₃-based electrode shows a single, clearly distinguishable exothermic peak at 287 °C with total enthalpy of 163 J g⁻¹ when charged up to 3.8 V. Charging up to a higher potential—4.5 V—led to an increase in the intensity of the decomposition peak and, correspondingly, the value of total enthalpy grew up to 239 J g⁻¹ (Table 1). In contrast to Na_{3-x}V₂(PO₄)₃, in the case of Na_{4-x}VMn(PO₄)₃, not only the “background” contribution of the surface reaction increased but also the intensity of the main peak (Figure 4), which was likely associated with the decomposition of the charged cathode material. It should be noted that in both cases, the charge up to 4.5 V provoked the splitting of the main exothermic peak into two proximate peaks. The results obtained indicate that Mn-substituted cathode material demonstrates much poorer thermal stability in their charged states, although pristine samples of both materials exhibit similar thermal behavior. Peak temperatures and thermal effect values for the cathode materials are shown in Table 1.

It is interesting to compare Na₃V₂(PO₄)₃- and Na₄VMn(PO₄)₃-based cathodes charged to 3.8 and 4.5 V in terms of the “heat on energy” factor introduced in a recent work [29].

The ratio of exothermic effect and the stored energy for the charged electrode material (both cathode or anode) may be estimated as $\text{HoE} = Q_{\text{rel}}/E_{\text{st}}$, where E_{st} is the specific energy gained upon charge of the material, and Q_{rel} is the heat released in DSC experiment (with both values given in the same units, e.g., $\text{J}\cdot\text{g}^{-1}$). The values of the HoE factor calculated for the studied materials are presented in Table 1. The data illustrates that $\text{Na}_3\text{V}_2(\text{PO}_4)_3$ charged to 3.8 V is the most efficient case from the point of view of “thermal efficiency”. However, $\text{Na}_4\text{VMn}(\text{PO}_4)_3$ demonstrates a lower HoE value when charged to 4.5 V, as compared with charging to 3.8 V. This is a consequence of a rather large increase in capacity and an average charging potential of above 3.8 V, in relation to the different heats released in DSC experiments.

In order to identify possible reasons for the different thermal behaviors of the electrodes, we analyzed the temperature-induced phase transformations of the initial and charged materials using in situ HTPXRD.

3.4. In Situ High-Temperature Powder X-ray Diffraction

The in situ HTPXRD patterns of the pristine and charged materials obtained within the 25–450 °C temperature range are shown in Figures 5 and 6, respectively. For the pristine $\text{Na}_3\text{V}_2(\text{PO}_4)_3$ and $\text{Na}_4\text{VMn}(\text{PO}_4)_3$ initial phosphates, no traces of thermal decomposition or phase transitions were observed. It is worth noting that there was an increase in the intensity of the peaks with increases in the temperature in an approximately reversible manner due to following possible reasons: (a) reversible structural changes caused by thermal expansion, (b) reversible structural changes caused by phase changing from C2/c (α -NVP) to $R\bar{3}c$ (γ -NVP) and (c) reversible increasing crystallinity caused by thermal expansion.

Both phosphates demonstrated a uniform shift of the positions of several reflections, indicating unit cell transformation. More precisely, parameter a remained almost constant, while parameter c grew with increasing temperatures. The shift of the positions of the 221 and 116 reflections can be seen in detail in Figure 5b; Figure 5c shows the anisotropic changes of lattice parameters. It should be noted that during the electrochemical charge-discharge [40,60], both parameters changed quite noticeably [67]. The a parameter declined on the course of Na^+ deintercalation for both $\text{Na}_3\text{V}_2(\text{PO}_4)_3$ and $\text{Na}_4\text{VMn}(\text{PO}_4)_3$. The c parameter of the $\text{Na}_3\text{V}_2(\text{PO}_4)_3$ contracted on the deintercalation of 2 Na^+ cations [45]. The c parameter of the $\text{Na}_4\text{VMn}(\text{PO}_4)_3$ reduced on the charge to 3.8 V and rapidly evolved on further charging [60]. Generally, it was the occupancy of the A1-site which was mainly responsible for the elongation of the NASICON unit cell predominantly in c direction [68].

In the case of thermal expansion, its anisotropy has previously been shown for other NASICON-type compounds [45–47,69–71]; Woodcock and Lightfoot suggest that it is caused by the temperature-induced redistribution of the A cations (Li, Na, K, Mg, etc.) between the A1 and A2 positions [72]. It cannot be the case for the room-temperature $\text{Na}_4\text{VMn}(\text{PO}_4)_3$ phase, since both positions are 100% occupied; however, high-temperature polymorphs of the NASICON-type compounds mentioned above have larger numbers of positions for Na atoms, so redistribution may take place [65]. The rate of thermal expansion in this case may be mainly governed by the thermal expansion of the $\text{A}^+\text{-O}$ bond and the radii of the constituent cations [68]. Still, the volume expansion of the $\text{Na}_3\text{V}_2(\text{PO}_4)_3$ and $\text{Na}_4\text{VMn}(\text{PO}_4)_3$ up to 450 °C is small and amounts to merely 1%.

Figure 6 illustrates HTPXRD patterns for the materials charged up to 3.8 V and 4.5 V cut-off potentials. Electrochemically desodiated $\text{Na}_3\text{V}_2(\text{PO}_4)_3$ demonstrates excellent thermal stability that follows from the absence of secondary phase reflections. No decrease in the intensity of the phase peaks, which could indicate amorphization of the material, was observed. However, in the case of the electrode charged to 3.8 V, reflections of the sodiated phase appeared at 400–450 °C, indicating the start of the thermal decomposition. The unit cell parameters of the reflections were close to the intermediate $\text{Na}_2\text{V}_2(\text{PO}_4)_3$ composition [73]. It is possible that if the electrode is charged up to 3.8 V, the $\text{Na}_3\text{V}_2(\text{PO}_4)_3 \rightarrow \text{NaV}_2(\text{PO}_4)_3$ phase transition is incomplete. The domains within the

material which retain the structure of the initial or metastable $\text{Na}_2\text{V}_2(\text{PO}_4)_3$ phases can, thus, act as the reaction centers of decomposition of the charged material. Residuals of the initial $\text{Na}_3\text{V}_2(\text{PO}_4)_3$ phase at 3.8 V are discussed in a previous paper [45].

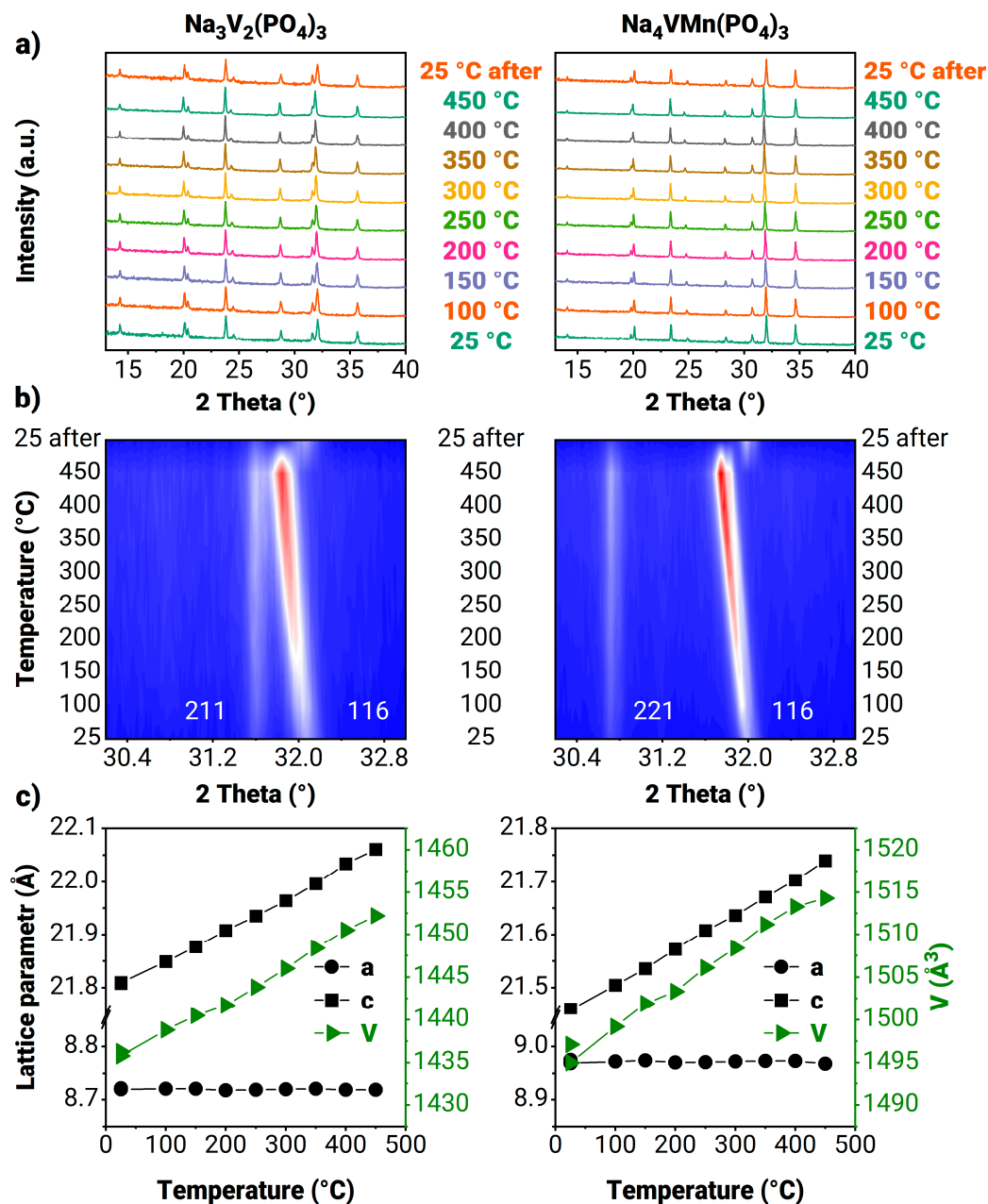


Figure 5. (a) In situ HTPXRD patterns for pristine powders of $\text{Na}_3\text{V}_2(\text{PO}_4)_3$ and $\text{Na}_4\text{VMn}(\text{PO}_4)_3$ cathode materials, (b) heat plot of 211 and 116 reflections (30.3–32.9°) and (c) lattice parameters.

HTPXRD data for the charged manganese-containing materials provided drastically different results. The decomposition process starts earlier in $\text{Na}_{4-x}\text{VMn}(\text{PO}_4)_3$ —in the temperature range of 150–200 °C. We observed no significant difference between the phase transformations of the material charged to 3.8 and 4.5 V. The variation in the structure decomposition temperature between in situ HTPXRD and DSC curves for $\text{Na}_{4-x}\text{VMn}(\text{PO}_4)_3$ might be associated with different experimental conditions; DSC experiments are performed under linear heating, whereas HTPXRD is carried out isothermally over ~4 h of exposure time. Moreover, it is well-known that the cathode-electrolyte interphase (CEI) is potential-sensitive, so charging up to 4.5 V triggers the formation of more reactive CEIs [74].

Hence, surface reactions are most likely responsible for the increase in the enthalpy of the decomposition of the phosphates charged up to 4.5 V. In contrast, powder X-ray diffraction (PXRD) registers a diffraction pattern for the bulk material of a crystalline solid, which results in a less prominent difference.

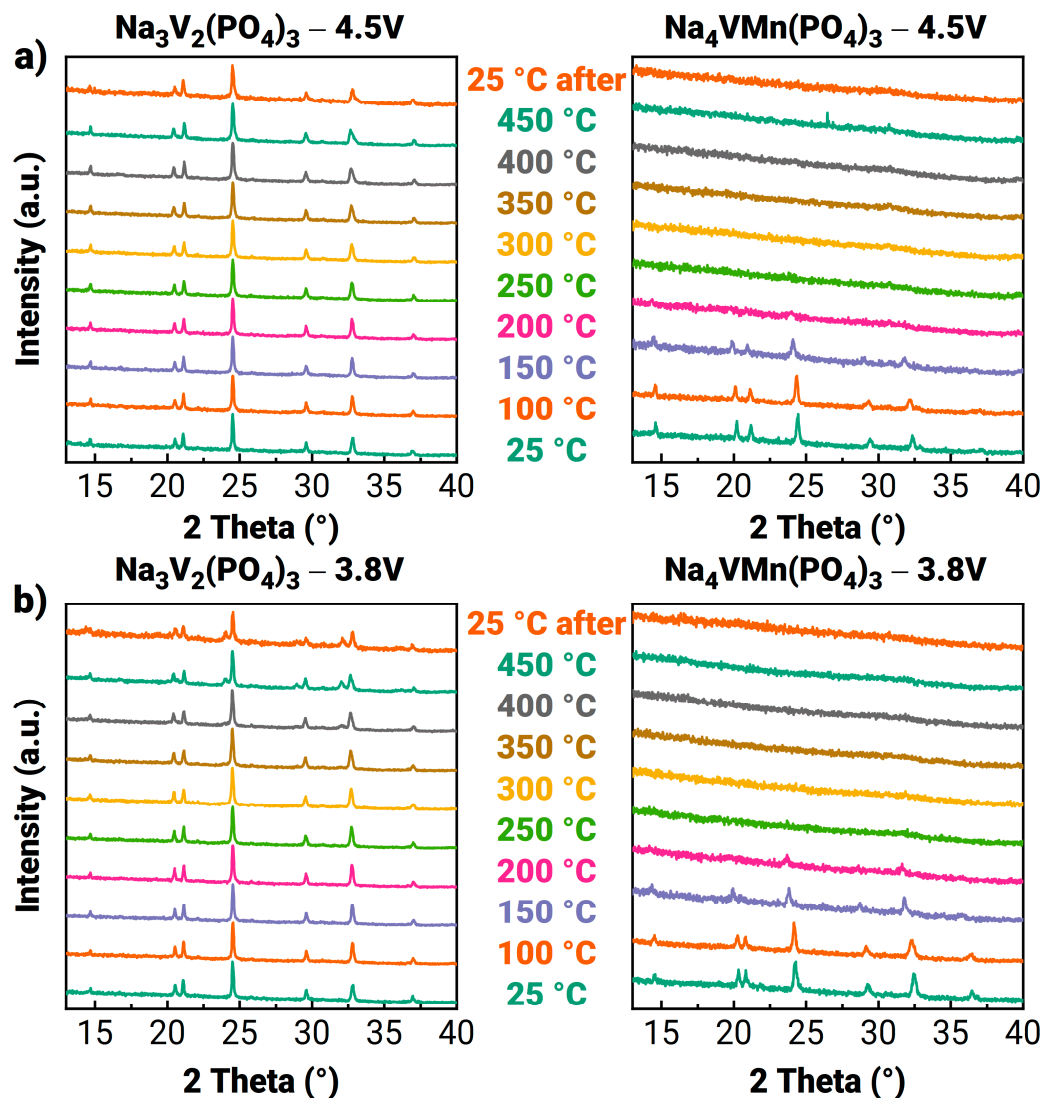


Figure 6. In situ HTPXRD patterns for the charged electrodes containing $\text{Na}_3\text{V}_2(\text{PO}_4)_3$ and $\text{Na}_4\text{VMn}(\text{PO}_4)_3$ cathode materials ((a) 4.5 V and (b) 3.8 V).

During decomposition, all the reflections vanish, which makes it impossible to perform the phase analysis of decomposition products through PXRD.

The results obtained indicate that the substitution of vanadium for manganese adversely affects the thermal stability of the NASICON-type materials in the charged state. A similar trend is observed by the authors who studied the substitution of iron for manganese in olivine-type LiMPO_4 [75–78]. Several groups report that delithiated $\text{Li}_{1-y}\text{FePO}_4$ cathode material is stable up to 450–500 °C, but $\text{Li}_{1-y}\text{MnPO}_4$ already starts to decompose at ~200 °C, which is accompanied by the formation of $\text{Mn}_2\text{P}_2\text{O}_7$ and oxygen release [75,76]. Kim et al. studied the thermal stability of $\text{Li}_{1-y}\text{Fe}_{1-x}\text{Mn}_x\text{PO}_4$ solid solutions ($x = 0.25, 0.5, 0.75$) and found that an increase in Mn content leads to a decrease in the decomposition temperature from ~500 °C for $x = 0.25$ to ~300 °C for $x = 0.75$ [75]. It should be noted that in their initial (lithiated) forms, LiMnPO_4 and LiFePO_4 show almost no difference in their thermal stability as well. The authors of the above-mentioned works agree that the instability

of delithiated Mn-containing olivines can be explained by the distortion of the structure caused by the Jahn–Teller effect, which is typical for Mn^{3+} . We can also suggest that the observed decrease in the thermal stability of the substituted $Na_{3+x}V_{2-x}Mn_x(PO_4)_3$ in its charged state and with an increase in manganese content is associated with the structural distortions introduced by Mn^{3+} cations as well [62].

4. Conclusions

In this work, we report on a systematic study of the thermal and phase transformation behavior of $Na_3V_2(PO_4)_3$ and $Na_4VMn(PO_4)_3$ cathode materials in their pristine and charged states and in the temperature range of 25–450 °C. Pristine materials have excellent thermal stability, which stems from the absence of exothermic effects and the formation of secondary phases. Upon heating, the thermal expansion of the NASICON unit cell proceeded mainly along the *c* axis in all studied phosphates. However, a distinct difference in thermal behavior was observed for the electrodes charged to 3.8 and 4.5 V vs. Na/Na⁺, compared to their pristine states. Desodiated $Na_{3-x}V_2(PO_4)_3$ also showed excellent thermal stability in the studied temperature range of 25–450 °C, but manganese substitution led to a decrease in the thermal stability of the charged material. According to DSC studies, desodiated $Na_{4-x}VMn(PO_4)_3$ demonstrates an almost twofold increase in decomposition enthalpy and lower onset temperatures for decomposition. In situ HTPXRD revealed the disappearance of the diffraction peaks of the desodiated $Na_{4-x}VMn(PO_4)_3$ at ~200 °C. Overall, the data obtained indicate that when tuning the composition of NASICON-type phosphates for practical application, it is necessary to consider not only the values of the potentials, capacity and energy density but also the changes in the thermal stability of materials.

Author Contributions: Conceptualization, R.R.S.; methodology, R.R.S.; investigation, R.R.S.; writing—original draft preparation, R.R.S.; writing—review and editing, M.V.Z., O.A.D. and E.V.A.; supervision, O.A.D. and E.V.A.; project administration, E.V.A.; funding acquisition, E.V.A. All authors have read and agreed to the published version of the manuscript.

Funding: This work was supported by the Russian Science Foundation (grant No. 17–73–30006–P).

Data Availability Statement: Not applicable.

Acknowledgments: This work was supported by the Interdisciplinary Scientific and Educational School of Moscow University’s “Future Planet and Global Environmental Change” program. We acknowledge Valeriy Yu. Verchenko for his support with the in situ high-temperature powder X-ray diffractions. We also acknowledge Grigory P. Lakienco for the fruitful discussions. The authors thank the Moscow State University Development program for granting us access to the LYNXEYE detector. R.R.S. is grateful to the Russian Foundation for Basic Research (young scientists’ grant, project No. 20–33–90161).

Conflicts of Interest: The authors declare no conflict of interest.

References

1. Cai, K.; Jing, X.; Zhang, Y.; Li, L.; Lang, X. A Novel Reed-Leaves like Aluminum-Doped Manganese Oxide Presetting Sodium-Ion Constructed by Coprecipitation Method for High Electrochemical Performance Sodium-Ion Battery. *Int. J. Energy Res.* **2022**, *46*, 14570–14580. [[CrossRef](#)]
2. Yang, L.; Wang, Q.; Liu, Y.; Luo, S.H.; Zhang, Y.; Liu, X. Optimize Solid-State Synthesis of P2-Na_{0.67}Ni_{0.33}Mn_{0.67}O₂ Cathode Materials by Using the Orthogonal Experimental Design Method. *Int. J. Energy Res.* **2021**, *45*, 16865–16873. [[CrossRef](#)]
3. Nwanya, A.C.; Ndipingwi, M.M.; Anthony, O.; Ezema, F.I.; Maaza, M.; Iwuoha, E.I. Impedance Studies of Biosynthesized Na_{0.8}Ni_{0.33}Co_{0.33}Mn_{0.33}O₂ Applied in an Aqueous Sodium-Ion Battery. *Int. J. Energy Res.* **2021**, *45*, 11123–11134. [[CrossRef](#)]
4. Chen, X.; Zhao, Z.; Huang, K.; Tang, H. Al-Substituted Stable-Layered P2-Na_{0.6}Li_{0.15}Al_{0.15}Mn_{0.7}O₂ Cathode for Sodium Ion Batteries. *Int. J. Energy Res.* **2021**, *45*, 11338–11345. [[CrossRef](#)]
5. Ponrouch, A.; Marchante, E.; Courty, M.; Tarascon, J.M.; Palacín, M.R. In Search of an Optimized Electrolyte for Na-Ion Batteries. *Energy Environ. Sci.* **2012**, *5*, 8572–8583. [[CrossRef](#)]
6. Tarascon, J.M. Na-Ion versus Li-Ion Batteries: Complementarity Rather than Competitiveness. *Joule* **2020**, *4*, 1616–1620. [[CrossRef](#)]

7. Hasa, I.; Mariyappan, S.; Saurel, D.; Adelhelm, P.; Kuposov, A.Y.; Masquelier, C.; Croguennec, L.; Casas-Cabanas, M. Challenges of Today for Na-Based Batteries of the Future: From Materials to Cell Metrics. *J. Power Sources* **2021**, *482*, 228872. [[CrossRef](#)]
8. Rudola, A.; Rennie, A.J.R.; Heap, R.; Meysami, S.S.; Lowbridge, A.; Mazzali, F.; Sayers, R.; Wright, C.J.; Barker, J. Commercialisation of High Energy Density Sodium-Ion Batteries: Faradion's Journey and Outlook. *J. Mater. Chem. A* **2021**, *9*, 8279–8302. [[CrossRef](#)]
9. Mikolajczak, C.; Kahn, M.; White, K.; Long, R.T. *Lithium-Ion Batteries Hazard and Use Assessment*; Springer Briefs in Fire; Springer: Boston, MA, USA, 2011; ISBN 978-1-4614-3485-6.
10. Verdianto, A.; Lim, H.; Kang, J.G.; Kim, S.O. Scalable, Colloidal Synthesis of SnSb Nanoalloy-Decorated Mesoporous 3D NiO Microspheres as a Sodium-Ion Battery Anode. *Int. J. Energy Res.* **2022**, *46*, 4267–4278. [[CrossRef](#)]
11. Saravanan, K.; Mason, C.W.; Rudola, A.; Wong, K.H.; Balaya, P.; Saravanan, K.; Mason, C.W.; Rudola, A.; Wong, K.H.; Balaya, P. The First Report on Excellent Cycling Stability and Superior Rate Capability of Na₃V₂(PO₄)₃ for Sodium Ion Batteries. *Adv. Energy Mater.* **2013**, *3*, 444–450. [[CrossRef](#)]
12. Zhu, L.; Sun, Q.; Xie, L.; Cao, X. Na₃V₂(PO₄)₃@NC Composite Derived from Polyaniline as Cathode Material for High-Rate and Ultralong-Life Sodium-Ion Batteries. *Int. J. Energy Res.* **2020**, *44*, 4586–4594. [[CrossRef](#)]
13. Jiang, Y.; Yang, Z.; Li, W.; Zeng, L.; Pan, F.; Wang, M.; Wei, X.; Hu, G.; Gu, L.; Yu, Y.; et al. Nanoconfined Carbon-Coated Na₃V₂(PO₄)₃ Particles in Mesoporous Carbon Enabling Ultralong Cycle Life for Sodium-Ion Batteries. *Adv. Energy Mater.* **2015**, *5*, 1402104. [[CrossRef](#)]
14. Ling, R.; Cai, S.; Xie, D.; Li, X.; Wang, M.; Lin, Y.; Jiang, S.; Shen, K.; Xiong, K.; Sun, X. Three-Dimensional Hierarchical Porous Na₃V₂(PO₄)₃/C Structure with High Rate Capability and Cycling Stability for Sodium-Ion Batteries. *Chem. Eng. J.* **2018**, *353*, 264–272. [[CrossRef](#)]
15. Li, Y.; Zhou, Q.; Weng, S.; Ding, F.; Qi, X.; Lu, J.; Li, Y.; Zhang, X.; Rong, X.; Lu, Y.; et al. Interfacial Engineering to Achieve an Energy Density of over 200 Wh Kg⁻¹ in Sodium Batteries. *Nat. Energy* **2022**, *7*, 511–519. [[CrossRef](#)]
16. Yan, G.; Mariyappan, S.; Rousse, G.; Jacquet, Q.; Deschamps, M.; David, R.; Mirvaux, B.; Freeland, J.W.; Tarascon, J.-M. Higher Energy and Safer Sodium Ion Batteries via an Electrochemically Made Disordered Na₃V₂(PO₄)₂F₃ Material. *Nat. Commun.* **2019**, *10*, 585. [[CrossRef](#)] [[PubMed](#)]
17. Bauer, A.; Song, J.; Vail, S.; Pan, W.; Barker, J.; Lu, Y. The Scale-up and Commercialization of Nonaqueous Na-Ion Battery Technologies. *Adv. Energy Mater.* **2018**, *8*, 1702869. [[CrossRef](#)]
18. Brant, W.R.; Mogensen, R.; Colbin, S.; Ojwang, D.O.; Schmid, S.; Hä Ggström, L.; Ericsson, T.; Jaworski, A.; Pell, A.J.; Younesi, R. Selective Control of Composition in Prussian White for Enhanced Material Properties. *Chem. Mater.* **2019**, *31*, 7203–7211. [[CrossRef](#)]
19. He, M.; Davis, R.; Chartouni, D.; Johnson, M.; Abplanalp, M.; Troendle, P.; Suetterlin, R.P. Assessment of the First Commercial Prussian Blue Based Sodium-Ion Battery. *J. Power Sources* **2022**, *548*, 232036. [[CrossRef](#)]
20. Jiang, X.; Zhang, T.; Lee, J.Y. Does Size Matter—What Other Factors Are Limiting the Rate Performance of Na₃V₂(PO₄)₃ Cathode in Sodium-Ion Batteries. *J. Power Sources* **2017**, *372*, 91–98. [[CrossRef](#)]
21. Essehli, R.; Alkhateeb, A.; Mahmoud, A.; Boschini, F.; Ben Yahia, H.; Amin, R.; Belharouak, I. Optimization of the Compositions of Polyanionic Sodium-Ion Battery Cathode NaFe_{2-x}V_x(PO₄)(SO₄)₂. *J. Power Sources* **2020**, *469*, 228417. [[CrossRef](#)]
22. Singh, B.; Wang, Z.; Park, S.; Gopalakrishnan, B.; Gautam, S.; El Chotard, J.-N.; Croguennec, L.; Carlier, D.; Cheetham, A.K.; Masquelier, C.; et al. A Chemical Map of NaSICON Electrode Materials for Sodium-Ion Batteries. *J. Mater. Chem. A* **2021**, *9*, 281–292. [[CrossRef](#)]
23. Li, H.; Jin, T.; Chen, X.; Lai, Y.; Zhang, Z.; Bao, W.; Jiao, L. Rational Architecture Design Enables Superior Na Storage in Greener NASICON-Na₄MnV(PO₄)₃ Cathode. *Adv. Energy Mater.* **2018**, *8*, 1801418. [[CrossRef](#)]
24. Hwang, J.; Matsumoto, K.; Hagiwara, R. Na₃V₂(PO₄)₃/C Positive Electrodes with High Energy and Power Densities for Sodium Secondary Batteries with Ionic Liquid Electrolytes That Operate across Wide Temperature Ranges. *Adv. Sustain. Syst.* **2018**, *2*, 1700171. [[CrossRef](#)]
25. Li, Z.; Dadsetan, M.; Gao, J.; Zhang, S.; Cai, L.; Naseri, A.; Jimenez-Castaneda, M.E.; Filley, T.; Miller, J.T.; Thomson, M.J.; et al. Revealing the Thermal Safety of Prussian Blue Cathode for Safer Nonaqueous Batteries. *Adv. Energy Mater.* **2021**, *11*, 202101764. [[CrossRef](#)]
26. Ojwang, D.O.; Häggström, L.; Ericsson, T.; Angström, J.; Brant, W.R. Influence of Sodium Content on the Thermal Behavior of Low Vacancy Prussian White Cathode Material. *Dalt. Trans.* **2020**, *49*, 3570–3579. [[CrossRef](#)]
27. Wang, K.; Huang, X.; Luo, C.; Zhang, Z.; Wang, H.; Zhou, T. Nanosheet-Assembled Hierarchical Petal-like Na₄MnV(PO₄)₃@Carbonized-Polyaniline Microspheres for Stable Sodium-Ion Batteries. *ACS Appl. Energy Mater.* **2022**. [[CrossRef](#)]
28. Zhang, X.; Zeng, M.; She, Y.; Lin, X.; Yang, D.; Qin, Y.; Rui, X. Enhanced Low-Temperature Sodium Storage Kinetics in a NaTi₂(PO₄)₃@C Nanocomposite. *J. Power Sources* **2020**, *477*, 228735. [[CrossRef](#)]
29. Samigullin, R.R.; Drozhzhin, O.A.; Antipov, E.V. Comparative Study of the Thermal Stability of Electrode Materials for Li-Ion and Na-Ion Batteries. *ACS Appl. Energy Mater.* **2022**, *5*, 14–19. [[CrossRef](#)]
30. Delmas, C.; Olazcuaga, R.; Cherkaoui, F.; Brochu, R.; Leflem, G. A New Family of Phosphates with Formula Na₃M₂(PO₄)₃ (M = Ti, V, Cr, Fe). *C. R. Seances Acad. Sci.* **1978**, *287*, 169–171.
31. Zatovsky, I.V. NASICON-Type Na₍₃₎V₍₂₎(PO₍₄₎)₍₃₎. *Acta Crystallogr. Sect. E Struct. Rep. Online* **2010**, *66*, i12. [[CrossRef](#)]

32. Jian, Z.; Zhao, L.; Pan, H.; Hu, Y.S.; Li, H.; Chen, W.; Chen, L. Carbon Coated $\text{Na}_3\text{V}_2(\text{PO}_4)_3$ as Novel Electrode Material for Sodium Ion Batteries. *Electrochem. Commun.* **2012**, *14*, 86–89. [[CrossRef](#)]
33. Shen, L.; Li, Y.; Roy, S.; Yin, X.; Liu, W.; Shi, S.; Wang, X.; Yin, X.; Zhang, J.; Zhao, Y. A Robust Carbon Coating of $\text{Na}_3\text{V}_2(\text{PO}_4)_3$ Cathode Material for High Performance Sodium-Ion Batteries. *Chin. Chem. Lett.* **2021**, *32*, 3570–3574. [[CrossRef](#)]
34. Chen, Y.; Xu, Y.; Sun, X.; Zhang, B.; He, S.; Li, L.; Wang, C. Preventing Structural Degradation from $\text{Na}_3\text{V}_2(\text{PO}_4)_3$ to $\text{V}_2(\text{PO}_4)_3$: F-Doped $\text{Na}_3\text{V}_2(\text{PO}_4)_3/\text{C}$ Cathode Composite with Stable Lifetime for Sodium Ion Batteries. *J. Power Sources* **2018**, *378*, 423–432. [[CrossRef](#)]
35. Wang, K.; Huang, X.; Zhou, T.; Sun, D.; Wang, H.; Zhang, Z. 3D Porous Spheroidal $\text{Na}_4\text{Mn}_{0.9}\text{Ce}_{0.1}\text{V}(\text{PO}_4)_3@ \text{CeO}_2/\text{C}$ Cathode for High-Energy Na Ion Batteries. *J. Mater. Chem. A* **2022**, *10*, 10625–10637. [[CrossRef](#)]
36. Wang, X.; Wang, W.; Zhu, B.; Qian, F.; Fang, Z. Mo-Doped $\text{Na}_3\text{V}_2(\text{PO}_4)_3@ \text{C}$ Composites for High Stable Sodium Ion Battery Cathode. *Front. Mater. Sci.* **2018**, *12*, 53–63. [[CrossRef](#)]
37. Li, H.; Tang, H.; Ma, C.; Bai, Y.; Alvarado, J.; Radhakrishnan, B.; Ong, S.P.; Wua, F.; Meng, Y.S.; Wu, C. Understanding the Electrochemical Mechanisms Induced by Gradient Mg^{2+} Distribution of Na-Rich $\text{Na}_3+\text{XV}_2-\text{XMg}_x(\text{PO}_4)_3/\text{C}$ for Sodium Ion Batteries. *Chem. Mater.* **2018**, *30*, 2498–2505. [[CrossRef](#)]
38. Chekannikov, A.; Kapaev, R.; Novikova, S.; Tabachkova, N.; Kulova, T.; Skundin, A.; Yaroslavtsev, A. $\text{Na}_3\text{V}_2(\text{PO}_4)_3/\text{C}/\text{Ag}$ Nanocomposite Materials for Na-Ion Batteries Obtained by the Modified Pechini Method. *J. Solid State Electrochem.* **2017**, *21*, 1615–1624. [[CrossRef](#)]
39. Aragón, M.J.; Lavela, P.; Ortiz, G.F.; Alcántara, R.; Tirado, J.L. Insight into the Electrochemical Sodium Insertion of Vanadium Superstoichiometric NASICON Phosphate. *Inorg. Chem.* **2017**, *56*, 11845–11853. [[CrossRef](#)]
40. Jian, Z.; Han, W.; Lu, X.; Yang, H.; Hu, Y.-S.; Zhou, J.; Zhou, Z.; Li, J.; Chen, W.; Chen, D.; et al. Superior Electrochemical Performance and Storage Mechanism of $\text{Na}_3\text{V}_2(\text{PO}_4)_3$ Cathode for Room-Temperature Sodium-Ion Batteries. *Adv. Energy Mater.* **2013**, *3*, 156–160. [[CrossRef](#)]
41. Zhu, W.; Wang, Y.; Liu, D.; Gariépy, V.; Gagnon, C.; Vijn, A.; Trudeau, M.L.; Zaghbi, K. Application of Operando X-Ray Diffractometry in Various Aspects of the Investigations of Lithium/Sodium-Ion Batteries. *Energies* **2018**, *11*, 2963. [[CrossRef](#)]
42. Aparicio, C.; Filip, J.; Machala, L. From Prussian Blue to Iron Carbides: High-Temperature XRD Monitoring of Thermal Transformation under Inert Gases. *Powder Diffr.* **2017**, *32*, S207–S212. [[CrossRef](#)]
43. Wang, W.; Gang, Y.; Peng, J.; Hu, Z.; Yan, Z.; Lai, W.; Zhu, Y.; Appadoo, D.; Ye, M.; Cao, Y.; et al. Effect of Eliminating Water in Prussian Blue Cathode for Sodium-Ion Batteries. *Adv. Funct. Mater.* **2022**, *32*, 2111727. [[CrossRef](#)]
44. Dai, H.; Yang, C.; Ou, X.; Liang, X.; Xue, H.; Wang, W.; Xu, G. Unravelling the Electrochemical Properties and Thermal Behavior of $\text{NaNi}_2/3\text{Sb}_1/3\text{O}_2$ Cathode for Sodium-Ion Batteries by in Situ X-Ray Diffraction Investigation. *Electrochim. Acta* **2017**, *257*, 146–154. [[CrossRef](#)]
45. Lim, S.Y.; Kim, H.; Shakoor, R.A.; Jung, Y.; Choi, J.W. Electrochemical and Thermal Properties of NASICON Structured $\text{Na}_3\text{V}_2(\text{PO}_4)_3$ as a Sodium Rechargeable Battery Cathode: A Combined Experimental and Theoretical Study. *J. Electrochem. Soc.* **2012**, *159*, A1393–A1397. [[CrossRef](#)]
46. Pet'kov, V.I.; Asabina, E.A.; Shchelokov, I.A. Thermal Expansion of NASICON Materials. *Inorg. Mater.* **2013**, *49*, 502–506. [[CrossRef](#)]
47. Forbes, R.P.; Barrett, D.H.; Rodella, C.B.; Billing, D.G. The Thermoresponsive Behaviour of Nasicon-like $\text{CuTi}_2(\text{PO}_4)_3$. *Mater. Charact.* **2019**, *155*, 109795. [[CrossRef](#)]
48. Cui, G.; Wang, H.; Yu, F.; Che, H.; Liao, X.; Li, L.; Yang, W.; Ma, Z. Scalable Synthesis of $\text{Na}_3\text{V}_2(\text{PO}_4)_3/\text{C}$ with High Safety and Ultrahigh-Rate Performance for Sodium-Ion Batteries. *Chin. J. Chem. Eng.* **2022**, *46*, 280–286. [[CrossRef](#)]
49. He, X.; Ping, P.; Kong, D.; Wang, G.; Wang, D. Comparison Study of Electrochemical and Thermal Stability of $\text{Na}_3\text{V}_2(\text{PO}_4)_3$ in Different Electrolytes under Room and Elevated Temperature. *Int. J. Energy Res.* **2022**, *46*, 23173–23194. [[CrossRef](#)]
50. Aragón, M.J.; Lavela, P.; Alcántara, R.; Tirado, J.L. Effect of Aluminum Doping on Carbon Loaded $\text{Na}_3\text{V}_2(\text{PO}_4)_3$ as Cathode Material for Sodium-Ion Batteries. *Electrochim. Acta* **2015**, *180*, 824–830. [[CrossRef](#)]
51. Aragón, M.J.; Lavela, P.; Ortiz, G.F.; Tirado, J.L. Effect of Iron Substitution in the Electrochemical Performance of $\text{Na}_3\text{V}_2(\text{PO}_4)_3$ as Cathode for Na-Ion Batteries. *J. Electrochem. Soc.* **2015**, *162*, A3077–A3083. [[CrossRef](#)]
52. Liu, R.; Xu, G.; Li, Q.; Zheng, S.; Zheng, G.; Gong, Z.; Li, Y.; Kruskop, E.; Fu, R.; Chen, Z.; et al. Exploring Highly Reversible 1.5-Electron Reactions ($\text{V}^{3+}/\text{V}^{4+}/\text{V}^{5+}$) in $\text{Na}_3\text{VCr}(\text{PO}_4)_3$ Cathode for Sodium-Ion Batteries. *ACS Appl. Mater. Interfaces* **2017**, *9*, 43632–43639. [[CrossRef](#)] [[PubMed](#)]
53. de Boisse, B.M.; Ming, J.; Nishimura, S.; Yamada, A. Alkaline Excess Strategy to NASICON-Type Compounds towards Higher-Capacity Battery Electrodes. *J. Electrochem. Soc.* **2016**, *163*, A1469–A1473. [[CrossRef](#)]
54. Zhou, W.; Xue, L.; Lü, X.; Gao, H.; Li, Y.; Xin, S.; Fu, G.; Cui, Z.; Zhu, Y.; Goodenough, J.B. $\text{Na}_x\text{MV}(\text{PO}_4)_3$ ($\text{M} = \text{Mn}, \text{Fe}, \text{Ni}$) Structure and Properties for Sodium Extraction. *Nano Lett.* **2016**, *16*, 7836–7841. [[CrossRef](#)]
55. Zakharkin, M.V.; Drozhzhin, O.A.; Ryazantsev, S.V.; Chernyshov, D.; Kirsanova, M.A.; Mikheev, I.V.; Pazhetnov, E.M.; Antipov, E.V.; Stevenson, K.J. Electrochemical Properties and Evolution of the Phase Transformation Behavior in the NASICON-Type $\text{Na}_{3+x}\text{MnxV}_{2-x}(\text{PO}_4)_3$ ($0 \leq x \leq 1$) Cathodes for Na-Ion Batteries. *J. Power Sources* **2020**, *470*, 228231. [[CrossRef](#)]
56. Anishchenko, D.V.; Zakharkin, M.V.; Nikitina, V.A.; Stevenson, K.J.; Antipov, E.V. Phase Boundary Propagation Kinetics Predominately Limit the Rate Capability of NASICON-Type $\text{Na}_{3+x}\text{MnxV}_{2-x}(\text{PO}_4)_3$ ($0 \leq x \leq 1$) Materials. *Electrochim. Acta* **2020**, *354*, 136761. [[CrossRef](#)]

57. Ghosh, S.; Barman, N.; Mazumder, M.; Pati, S.K.; Rousse, G.; Senguttuvan, P. High Capacity and High-Rate NASICON- $\text{Na}_{3.75}\text{V}_{1.25}\text{Mn}_{0.75}(\text{PO}_4)_3$ Cathode for Na-Ion Batteries via Modulating Electronic and Crystal Structures. *Adv. Energy Mater.* **2019**, *10*, 1902918. [CrossRef]
58. Cui, G.; Dong, Q.; Wang, Z.; Liao, X.Z.; Yuan, S.; Jiang, M.; Shen, Y.; Wang, H.; Che, H.; He, Y.S.; et al. Achieving Highly Reversible and Fast Sodium Storage of $\text{Na}_4\text{VMn}(\text{PO}_4)_3/\text{C-RGO}$ Composite with Low-Fraction RGO via Spray-Drying Technique. *Nano Energy* **2021**, *89*, 106462. [CrossRef]
59. Gao, X.; Lian, R.; He, L.; Fu, Q.; Indris, S.; Schwarz, B.; Wang, X.; Chen, G.; Ehrenberg, H.; Wei, Y. Phase Transformation, Charge Transfer, and Ionic Diffusion of $\text{Na}_4\text{MnV}(\text{PO}_4)_3$ in Sodium-Ion Batteries: A Combined First-Principles and Experimental Study. *J. Mater. Chem. A* **2020**, *8*, 17477–17486. [CrossRef]
60. Chen, F.; Kovrugin, V.M.; David, R.; Mentré, O.; Fauth, F.; Chotard, J.-N.; Masquelier, C. A NASICON-Type Positive Electrode for Na Batteries with High Energy Density: $\text{Na}_4\text{MnV}(\text{PO}_4)_3$. *Small Methods* **2018**, *3*, 1800218. [CrossRef]
61. Buryak, N.S.; Anishchenko, D.V.; Levin, E.E.; Ryazantsev, S.V.; Martin-Diaconescu, V.; Zakharkin, M.V.; Nikitina, V.A.; Antipov, E.V. High-Voltage Structural Evolution and Its Kinetic Consequences for the $\text{Na}_4\text{MnV}(\text{PO}_4)_3$ Sodium-Ion Battery Cathode Material. *J. Power Sources* **2022**, *518*, 230769. [CrossRef]
62. Ghosh, S.; Barman, N.; Patra, B.; Senguttuvan, P. Structural and Electrochemical Sodium (De)Intercalation Properties of Carbon-Coated NASICON- $\text{Na}_{3+y}\text{V}_{2-y}\text{Mn}_y(\text{PO}_4)_3$ Cathodes for Na-Ion Batteries. *Adv. Energy Sustain. Res.* **2022**, *3*, 2200081. [CrossRef]
63. Zakharkin, M.V.; Drozhzhin, O.A.; Tereshchenko, I.V.; Chernyshov, D.; Abakumov, A.M.; Antipov, E.V.; Stevenson, K.J. Enhancing Na^+ Extraction Limit through High Voltage Activation of the NASICON-Type $\text{Na}_4\text{MnV}(\text{PO}_4)_3$ Cathode. *ACS Appl. Energy Mater.* **2018**, *1*, 5842–5846. [CrossRef]
64. Zhang, J.; Zhao, X.; Song, Y.; Li, Q.; Liu, Y.; Chen, J.; Xing, X. Understanding the Superior Sodium-Ion Storage in a Novel $\text{Na}_{3.5}\text{Mn}_{0.5}\text{V}_{1.5}(\text{PO}_4)_3$ Cathode. *Energy Storage Mater.* **2019**, *23*, 25–34. [CrossRef]
65. Chotard, J.N.; Rousse, G.; David, R.; Mentré, O.; Courty, M.; Masquelier, C. Discovery of a Sodium-Ordered Form of $\text{Na}_3\text{V}_2(\text{PO}_4)_3$ below Ambient Temperature. *Chem. Mater.* **2015**, *27*, 5982–5987. [CrossRef]
66. Zhou, Q.; Li, Y.; Tang, F.; Li, K.; Rong, X.; Lu, Y.; Chen, L.; Hu, Y.-S. Thermal Stability of High Power 26650-Type Cylindrical Na-Ion Batteries. *Chin. Phys. Lett.* **2021**, *38*, 076501. [CrossRef]
67. Perfil'yeva, T.I.; Drozhzhin, O.A.; Alekseeva, A.M.; Zakharkin, M.V.; Mironov, A.V.; Mikheev, I.V.; Bobyleva, Z.V.; Marenko, A.P.; Marikutsa, A.V.; Abakumov, A.M.; et al. Complete Three-Electron Vanadium Redox in NASICON-Type $\text{Na}_3\text{VSc}(\text{PO}_4)_3$ Electrode Material for Na-Ion Batteries. *J. Electrochem. Soc.* **2021**, *168*, 110550. [CrossRef]
68. Pet'kov, V.I.; Orlova, A.I. Crystal-Chemical Approach to Predicting the Thermal Expansion of Compounds in the NZP Family. *Inorg. Mater.* **2003**, *39*, 1013–1023. [CrossRef]
69. Deng, Y.; Eames, C.; Nguyen, L.H.B.; Pecher, O.; Griffith, K.J.; Courty, M.; Fleutot, B.; Chotard, J.N.; Grey, C.P.; Islam, M.S.; et al. Crystal Structures, Local Atomic Environments, and Ion Diffusion Mechanisms of Scandium-Substituted Sodium Superionic Conductor (NASICON) Solid Electrolytes. *Chem. Mater.* **2018**, *30*, 2618–2630. [CrossRef]
70. Qui, D.T.; Capponi, J.J.; Joubert, J.C.; Shannon, R.D. Crystal Structure and Ionic Conductivity in $\text{Na}_4\text{Zr}_2\text{Si}_3\text{O}_{12}$. *J. Solid State Chem.* **1981**, *39*, 219–229. [CrossRef]
71. Huang, C.Y.; Agrawal, D.K.; McKinstry, H.A. Thermal Expansion Behaviour of $M'\text{Ti}_2\text{P}_3\text{O}_{12}$ ($M'=\text{Li, Na, K, Cs}$) and $M''\text{Ti}_4\text{P}_6\text{O}_{24}$ ($M''=\text{Mg, Ca, Sr, Ba}$) Compounds. *J. Mater. Sci.* **1995**, *30*, 3509–3514. [CrossRef]
72. Woodcock, D.A.; Lightfoot, P. Comparison of the Structural Behaviour of the Low Thermal Expansion NZP Phases $\text{MTi}_2(\text{PO}_4)_3$ ($M = \text{Li, Na, K}$). *J. Mater. Chem.* **1999**, *9*, 2907–2911. [CrossRef]
73. Park, S.; Wang, Z.; Deng, Z.; Moog, I.; Canepa, P.; Fauth, F.; Carlier, D.; Croguennec, L.; Masquelier, C.; Chotard, J.-N. Crystal Structure of $\text{Na}_2\text{V}_2(\text{PO}_4)_3$, an Intriguing Phase Spotted in the $\text{Na}_3\text{V}_2(\text{PO}_4)_3\text{--Na}_1\text{V}_2(\text{PO}_4)_3$ System. *Chem. Mater.* **2022**, *34*, 451–462. [CrossRef]
74. Gauthier, M.; Carney, T.J.; Grimaud, A.; Giordano, L.; Pour, N.; Chang, H.H.; Fenning, D.P.; Lux, S.F.; Paschos, O.; Bauer, C.; et al. Electrode-Electrolyte Interface in Li-Ion Batteries: Current Understanding and New Insights. *J. Phys. Chem. Lett.* **2015**, *6*, 4653–4672. [CrossRef] [PubMed]
75. Kim, J.; Park, K.Y.; Park, I.; Yoo, J.K.; Hong, J.; Kang, K. Thermal Stability of Fe-Mn Binary Olivine Cathodes for Li Rechargeable Batteries. *J. Mater. Chem.* **2012**, *22*, 11964–11970. [CrossRef]
76. Yoshida, J.; Nakanishi, S.; Iba, H.; Abe, H.; Naito, M. Thermal Behavior of Delithiated $\text{Li}_1\text{-xMnPO}_4$ ($0 \leq x < 1$) Structure for Lithium-Ion Batteries. *Int. J. Appl. Ceram. Technol.* **2013**, *10*, 764–772. [CrossRef]
77. Huang, Y.; Lin, Y.C.; Jenkins, D.M.; Chernova, N.A.; Chung, Y.; Radhakrishnan, B.; Chu, I.H.; Fang, J.; Wang, Q.; Omenya, F.; et al. Thermal Stability and Reactivity of Cathode Materials for Li-Ion Batteries. *ACS Appl. Mater. Interfaces* **2016**, *8*, 7013–7021. [CrossRef]
78. Chen, G.; Richardson, T.J. Thermal Instability of Olivine-Type LiMnPO_4 Cathodes. *J. Power Sources* **2010**, *195*, 1221–1224. [CrossRef]

Disclaimer/Publisher's Note: The statements, opinions and data contained in all publications are solely those of the individual author(s) and contributor(s) and not of MDPI and/or the editor(s). MDPI and/or the editor(s) disclaim responsibility for any injury to people or property resulting from any ideas, methods, instructions or products referred to in the content.